Final shape of a drying thin film

Tohru Okuzono, Masaru Kobayashi, and Masao Doi
Department of Applied Physics, The University of Tokyo, Tokyo 113-8656, Japan
(Received 19 March 2009; published 12 August 2009)

Drying processes of polymer solutions on a solid substrate enclosed by bank are studied in the slow limit of the solvent evaporation. A simple model is proposed to examine the final shape of the film after drying. Analytical expressions of the final shape in terms of the initial parameters are obtained. It is shown that the craterlike and basinlike shapes appear as final shapes of the film depending on the initial parameters. The "shape diagrams" which show parameter dependence of the final shape are presented in the absence/presence of diffusion. The final shape of the film in the geometry without bank is also discussed.

DOI: 10.1103/PhysRevE.80.021603 PACS number(s): 68.03.Fg, 82.70.Gg, 68.35.Fx

I. INTRODUCTION

Drying of thin liquid films or droplets placed on a solid substrate is an everyday-life phenomenon, but its dynamics is rather complex and involves many challenging problems in soft matter physics, such as the coffee stain problems [1–9], motion and pinning of contact lines [10–14], pattern formation of deposits [15–19], effects of inhomogeneous surface tension (Marangoni effect) [20–25], skin formation [26–29], and buckling instabilities [30–33]. The problem is also very important in various industrial applications, such as manufacturing polymer films [34–36], inkjet printing [37,38], and other printing and coating technologies. Various investigations [34–43] have also been done from this engineering viewpoint.

For the industrial applications, an important problem is how to control the shape of the final deposit left after the liquid film which is a mixture of volatile solvent and nonvolatile solute (polymers or colloid particles) is dried. It is known that the shape depends on the dynamics of the drying process. If the evaporation of solvent is very fast, the solute concentration near the surface increases rapidly and a "skin," a thin gel-like phase near the surface, appears [26,28]. In this case, the deposit shape is essentially determined by the growth of the skin phase. On the other hand, if the evaporation is slow, the internal flow within the liquid phase plays the major role. Deegan *et al.* [1] pointed out that the flow induced by the solvent evaporation transports the solute toward the edge (contact line) of the liquid and that this creates a ringlike pattern of the deposit, the so-called coffee ring.

Systematic studies for the shape of the deposit of polymer solution were conducted by Jung *et al.* [43]. They studied the simplest case where (1) the contact line is pinned and (2) the polymer solution can be regarded as Newtonian fluid. Even with such simplification, they showed that the shape of the final deposit changes from moundlike, craterlike, and basinlike depending on the initial polymer concentration and the initial volume of the film.

It has been a challenge to predict the final shape of the deposit by computer simulation. So far, the modeling has been done only for the case of slow evaporation (the case of flow dominant regime). Ozawa *et al.* [41] proposed a model for the drying dynamics of a polymer solution droplet on a substrate taking the effects of the gelation (or solidification) into account. The model involves a set of nonlinear partial differential equations and requires numerical calculation for the analysis. Accordingly, it is not clear which parameter determines the final shape of the deposit.

In this paper, we shall propose a simple model by which we can conduct the analysis almost analytically (or with small numerical computation). The aim of this model is to clarify the parameters which are relevant to giving the final shape and to predict the shape in terms of the parameters. To our knowledge, there have been no analytical theories to predict the final shape of the drying film. We present in this paper a detailed analysis which predicts that there are three types of the final shape depending on the initial parameters concerned with the initial height of the film and the initial polymer concentration, which is consistent with the recent experimental results [43].

The construction of this paper is as follows. In Sec. II, we describe our model. In Sec. III we analyze the model theoretically in the limit that the diffusion effect of polymer is negligible and construct the "shape diagram" which predicts the type of the deposit shape in terms of the initial parameters. We also show the shape diagrams for the case that the diffusion effect is non-negligible. In Sec. IV we discuss the result for the bankless case. Finally, we summarize our results and conclude this paper.

II. MODEL

A. Conservation laws

Consider drying of polymer solution on a solid substrate enclosed by "bank" as illustrated in Fig. 1. The system is in two dimensions with the horizontal coordinate x along the substrate and the vertical coordinate z. The gas-liquid interface $z=h(x,t)$ is pinned at the contact points $(\pm l_0,h_0)$ at any time t. Suppose that the system is isothermal and the latent heat effects [44] can be ignored and that the aspect ratio of the system is sufficiently small, that is, $h_0/l_0 \ll 1$, where l_0 is a size of the system and h_0 is a height of the bank. We assume that the diffusion length l_d of the polymer concentration ϕ is much larger than the film thickness and much smaller than the system size, i.e., $h_0 \ll l_d \ll l_0$. Therefore, the variation in ϕ in z direction is negligible so that the concentration ϕ can be regarded as a function of x and time t: $\phi = \phi(x,t)$.

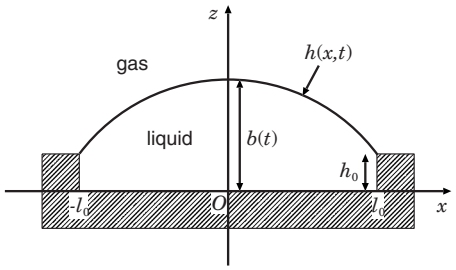

FIG. 1. Geometry and coordinates of our model system. A polymer solution is spread on a solid substrate enclosed by banks whose height is h_0 and the solvent evaporates from the free surface at $z=h(x,t)$.

Under the above assumptions we can express the local conservations of solvent and solute as a couple of continuity equations:

$$\frac{\partial h}{\partial t} + \frac{\partial Q}{\partial x} = -J, \tag{1}$$

$$\frac{\partial}{\partial t}(\phi h) + \frac{\partial}{\partial x}(\phi Q) = \frac{\partial}{\partial x}\left(Dh\frac{\partial \phi}{\partial x}\right), \tag{2}$$

where $h=h(x,t)$ is the height of the free surface, $J=J(x,t)$ is the solvent evaporation rate which is a function of x and t, in general, D is the diffusion coefficient, and $Q=Q(x,t)$ is the volume flux defined as

$$Q(x,t) \equiv \int_0^{h(x,t)} u(x,z,t)dz, \tag{3}$$

with $u(x,z,t)$ as the x component of fluid velocity.

The above model is valid for the following situations. Since the incompressibility of the fluid implies that $\partial u/\partial x \sim J_0/h_0$ with a characteristic value J_0 of J, the magnitude of the mean velocity of the fluid is of the order of $J_0 l_0/h_0$ and the characteristic time can be estimated as h_0/J_0. Hence the diffusion length l_d can be estimated as $(Dh_0/J_0)^{1/2}$. Therefore the condition that Eq. (2) is valid is $1 \ll D/(J_0 h_0) \ll (l_0/h_0)^2$. This condition is satisfied in practical situations. Indeed, the typical experimental values [43] ($D \sim 3\times 10^{-11}$ m^2/s, $J_0 \sim 5\times 10^{-8}$ m/s, $h_0 \sim 2\times 10^{-6}$ m, and $l_0 \sim 2\times 10^{-4}$ m) lead to $D/(J_0 h_0) \sim 3\times 10^2$ and $(l_0/h_0)^2 \sim 10^4$.

From Eqs. (1) and (2), we obtain

$$h\frac{\partial \phi}{\partial t} + Q\frac{\partial \phi}{\partial x} = \frac{\partial}{\partial x}\left(Dh\frac{\partial \phi}{\partial x}\right) + J\phi. \tag{4}$$

Equations (1) and (2), or equivalently, Eqs. (1) and (4), are basic equations which describe the time evolution of the shape of the film and the concentration of polymers in the drying films. However, Q and J are still unknown. We will give expressions to these quantities below.

B. Simplification of the problem

In the case that $h(x,t)$ slowly varies in x ($\partial h/\partial x \sim h_0/l_0 \ll 1$), it is usual to use the lubrication approximation for Newtonian fluids [45]. This gives the following expression for the flux $Q(x,t)$,

$$Q(x,t) = \frac{\gamma}{3\eta}h^3\frac{\partial^3 h}{\partial x^3}, \tag{5}$$

where γ is the interfacial tension between the gas and the liquid and η is the shear viscosity of the liquid.

The evaporation rate $J(x,t)$ can be derived from the flux of the solvent in the gas phase near the gas-liquid interface. The flux should be determined by solving the diffusion equation of the solvent concentration in the gas phase under the boundary conditions which depend on the polymer concentration ϕ in the liquid phase near the interface [26,29].

The above argument leads to a complex moving boundary problem of nonlinear partial differential equations. It is possible to carry out a numerical simulation of Eqs. (1) and (2) using Eq. (5) together with the diffusion equation of the solvent concentration in the gas phase to obtain the evaporation rate [46]. However, it is difficult to have an overview by such numerical simulations. In order to see how the final shape is affected when the drying conditions are changed, it is preferable to have a simple analytical theory. In the following, we shall construct such a theory.

For our purpose of predicting the final shape qualitatively, we take into account only what we think the essential points of the drying process. These are the following: (i) the evaporation induces the outward flow [1] in the liquid phase which transports the solute to the edge of the system. (ii) The flow of the liquid and the evaporation of the solvents are strongly suppressed when the polymer concentration ϕ reaches a certain value ϕ_g, which we call the "gelation concentration." Notice that ϕ_g is not a rigorously defined concentration: it is a concentration at which the viscosity increases sharply [41,43] and the elastic effect of the solution becomes important [29]. Taking these facts into account, we simplify the problem under the assumptions below.

The first assumption is that the evaporation rate J_0 is much smaller than the velocity γ/η induced by the capillary force, that is, $\mathrm{Ca} \to 0$, where the capillary number Ca is defined as

$$\mathrm{Ca} \equiv \frac{\eta J_0}{\gamma}. \tag{6}$$

In this case $h(x,t)$ will be close to an equilibrium shape at each time. Hence we can make an approximation, instead of solving Eq. (1) with Eq. (5), as

$$h(x,t) = -a(t)x^2 + b(t). \tag{7}$$

This is a crude approximation for the shape evolution. (For more general cases, see Appendix A.) The time-dependent coefficients $a(t)$ and $b(t)$ in Eq. (7) should be determined by the conservation law Eq. (1) with a geometrical condition at the edges of the system.

The second assumption is that the evaporation rate is constant in the solution phase, whereas it vanishes in the gel phase, that is,

$$J(x,t) = \begin{cases} J_0 & (\text{in solution}), \\ 0 & (\text{in gel}). \end{cases} \tag{8}$$

Moreover, we assume that $\phi=\phi_g$ and $Q=0$ in the gel phase.

As we mentioned above, the evaporation rate should be determined by solving the diffusion equation in the gas phase, which may lead to a divergence of J at the edges of the liquid region in a certain situation. However, this divergence might be suppressed when the edges are gelation fronts because J depends on ϕ at the gas-liquid interface and considerably decreases as ϕ approaches ϕ_g [29]. We cannot specify an explicit functional form of $J(x,t)$ without solving the diffusion equation in the gas phase. Therefore, it might be acceptable, as a first step, to assume the uniform evaporation rate in order to see an effect of the outward flow induced by pinning of the contact points on the shape of the final deposit. It should be noted that the divergence of J at the edges enhances the outward flow but is not expected to change qualitatively our results shown in this paper. The divergence of J should play an important role in the motion of contact lines [10–14] and other phenomena, which is out of the scope of the present paper.

C. Simplified model

1. Pregelation regime

Here we describe our model in the early time regime where a gel-like phase does not appear ($\phi < \phi_g$). Integrating Eq. (1) over $[0,x]$ after substitution of Eq. (7) into Eq. (1), the conditions $Q(0,t)=Q(l_0,t)=0$ lead to

$$\frac{da}{dt} = -\frac{3}{2l_0^3}\mathcal{J}(l_0,t), \tag{9}$$

where

$$\mathcal{J}(x,t) \equiv \int_0^x dx' J(x',t) \tag{10}$$

is the integrated evaporation rate. Here we have used the relation $h_0=-a(t)l_0^2+b(t)$. Then we have

$$Q(x,t) = \frac{\bar{J}(t)}{2}x\left(1-\frac{x^2}{l_0^2}\right) - \delta\mathcal{J}(x,t), \tag{11}$$

where

$$\bar{J}(t) \equiv \frac{1}{l_0}\int_0^{l_0} dx J(x,t) \tag{12}$$

and

$$\delta\mathcal{J}(x,t) \equiv \int_0^x dx'[J(x',t)-\bar{J}(t)]. \tag{13}$$

With the second assumption in the previous section, we ignore the inhomogeneity of the evaporation rate $\delta\mathcal{J}(x,t)$ and the time dependence of $\bar{J}(t)$. Then we have, putting $\bar{J}(t)=J_0$ with a constant $J_0 \geq 0$,

$$Q(x,t) = \frac{J_0}{2}x\left(1-\frac{x^2}{l_0^2}\right), \tag{14}$$

and

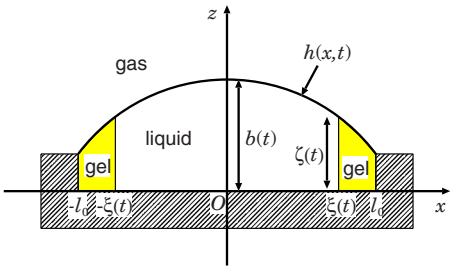

FIG. 2. (Color online) Schematic of the model system in the postgelation regime. The gel phase region $[\xi(t) \leq x \leq l_0]$ begins to develop from the edge ($x=l_0$).

$$a(t) = a_0 - \frac{3}{2l_0^2}J_0 t, \tag{15}$$

$$b(t) = b_0 - \frac{3}{2}J_0 t, \tag{16}$$

with initial values a_0 and b_0 for $a(t)$ and $b(t)$, respectively.

Note that $Q(x,t)$ which leads to the so-called outward flow is independent of time in this case (the mean flow Q/h depends on time). It should be emphasized that the outward flow is a result of the pinning of contact points and exists even if the evaporation rate is uniform. The time evolution of $\phi(x,t)$ is described by Eq. (4) with Eqs. (7) and (14)–(16).

2. Postgelation regime

In the above model, the mass of polymers will move toward the edges of the system ($x=\pm l_0$) due to the outward flow. We can expect in most cases that the concentration of polymers at $x=l_0$ rapidly increases and reaches the gelation concentration ϕ_g above which a gel-like phase appears. In the following, we restrict ourselves to considering the case that the gel phase region begins to develop from the edge so that the position $x=\xi(t)$ of the gelation front at time t monotonically decreases from $\xi=l_0$ to 0 (see Fig. 2). (Hereafter we consider the region $x \geq 0$ only due to the symmetry.) In some parameter region, however, the gelation may take place at the center ($x=0$). In this case we can switch to another model shown in Appendix A and will use the model in the following numerical simulations.

The second assumption in the previous section reads in this case

$$J(x,t) = \begin{cases} J_0 & [0 \leq x < \xi(t)] \\ 0 & [\xi(t) \leq x \leq l_0], \end{cases} \tag{17}$$

and

$$\phi(x,t) = \phi_g, \quad [\xi(t) \leq x \leq l_0]. \tag{18}$$

Furthermore we assume that $Q(x,t)=0$ in the gel phase. Then we obtain

$$Q(x,t) = \begin{cases} \dfrac{J_0}{2}x\left(1-\dfrac{x^2}{\xi^2}\right) & [0 \leq x < \xi(t)] \\ 0 & [\xi(t) \leq x \leq l_0], \end{cases} \tag{19}$$

provided that $\xi(t)$ is given.

Let

$$\zeta(t) \equiv h(\xi,t) \tag{20}$$

be the height of the film at the gelation front $x=\xi(t)$ at time t. Because of the geometrical constraint at $x=\xi$, Eq. (7) can be written as

$$h(x,t) = -(b-\zeta)\frac{x^2}{\xi^2} + b, \quad (0 \le x \le \xi), \tag{21}$$

where b is given by Eq. (16) which still holds after the gelation occurs. From Eqs. (4) and (17)–(21), and the boundary condition $\partial\phi/\partial x=0$ at $x=0$, we can determine a trajectory of $[\xi(t),\zeta(t)]$ that is a final shape of the film after drying.

Note that conservation of the total amount of polymers implies

$$Dh(x,t)\frac{\partial\phi}{\partial x} = Q(x,t)\phi(x,t), \quad [x\uparrow\xi(t)]. \tag{22}$$

This means that $\partial\phi/\partial x=0$ at $x=\xi(t)$ for finite D because of $Q(\xi,t)=0$.

III. THEORETICAL AND NUMERICAL ANALYSES

In this section, we analyze the simplified model given in the previous section. In the case that the diffusion effect is negligible ($D=0$), we can solve the problem analytically and can predict the final shape of the drying film in terms of initial shape and concentration of the polymer solution. If the diffusion is non-negligible, it gives a correction to this result.

The mathematical problems to be solved in our model are summarized as follows. For $D=0$, we solve the initial value problems of the first-order partial differential Eq. (4) in the two time regions: (a) in the pregelation regime $0<t<t_g$ with the gelation time t_g (see the next section), we solve Eq. (4) with Eqs. (7) and (14)–(16) for the initial value $\phi(x,0)=\phi_0$ with a constant ϕ_0. (b) In the postgelation regime $t>t_g$, we solve Eq. (4) with Eqs. (21) and (16)–(20) for the initial value $\phi(x,t_g)=\tilde{\phi}(x)$ given as a solution of the problem (a). In these cases boundary conditions are not necessary. For the numerical calculations, however, we need the boundary condition $\partial\phi/\partial x=0$ at $x=0$ due to the symmetry.

For $D\neq 0$, we solve the boundary value problems of the second-order partial differential Eq. (4) in the two time regions: (c) in the pregelation regime $0<t<t_g$, we solve Eq. (4) with Eqs. (7) and (14)–(16) under the boundary conditions $\partial\phi/\partial x=0$ at $x=0$ and l_0 for the initial value $\phi(x,0)=\phi_0$. (d) In the postgelation regime $t>t_g$, we solve Eq. (4) with Eqs. (21) and (16)–(20) under the boundary conditions $\partial\phi/\partial x=0$ at $x=0$ and $\xi(t)$ for the initial value $\phi(x,t_g)=\tilde{\phi}(x)$ given as a solution of the problem (c).

The method which will be shown below can be applied for the system with the axial symmetry. The main results of the analysis for that system are presented in Appendix B.

A. No diffusion case

1. Numerical simulation

Before the theoretical analysis, we show some results of numerical simulations of the simplified model. In this section we choose l_0, h_0, and h_0/J_0 as units of space in x direction, that in z direction, and time, respectively. In these units, Eq. (4) without the diffusion term is written as

$$h\frac{\partial\phi}{\partial t} + Q\frac{\partial\phi}{\partial x} = J\phi, \tag{23}$$

where h, Q, and J are now the dimensionless functions given by the same expression of Eq. (7) or Eq. (21) with

$$a(t) = a_0 - \frac{3}{2}t, \tag{24}$$

$$b(t) = b_0 - \frac{3}{2}t, \tag{25}$$

$$Q(x,t) = \begin{cases} \dfrac{x}{2}\left(1-\dfrac{x^2}{\xi^2}\right) & [0 \le x < \xi(t)] \\ 0 & [\xi(t) \le x \le 1], \end{cases} \tag{26}$$

and

$$J(x,t) = \begin{cases} 1 & [0 \le x < \xi(t)] \\ 0 & [\xi(t) \le x \le 1]. \end{cases} \tag{27}$$

In the above expressions we should understand $\xi=\zeta=1$ in the pregelation regime.

In the pregelation regime, we numerically solve Eq. (23) with Eqs. (7) and (24)–(27) under the boundary condition $\partial\phi/\partial x=0$ at $x=0$ for the initial state $\phi(x,0)=\phi_0$ with a constant ϕ_0. When the gelation starts, we switch to the postgelation model [alternatively using Eqs. (A1)–(A5)] and we obtain a final shape of the film as a trajectory of $[\xi(t),\zeta(t)]$. In Fig. 3 we show typical profiles of drying film at three different times. In the liquid region ($x<\xi$) the profile is expressed as Eq. (21) and in the gel region ($\xi \le x<1$) it is a part of the trajectory of $[\xi(t),\zeta(t)]$. It can be shown that

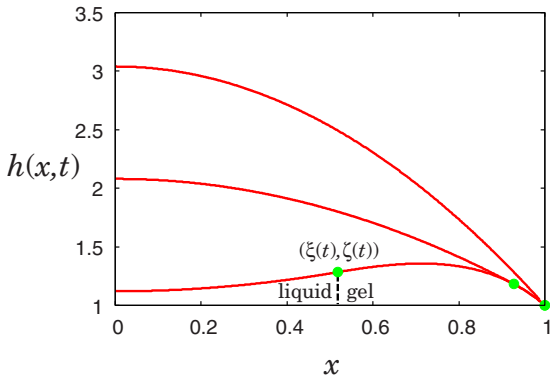

FIG. 3. (Color online) Typical time evolution of the profile of $h(x,t)$ in the liquid region and that of the deposit in the gel region. Solid lines show the total profiles of drying films in both liquid and gel region. The three solid lines correspond to the different times (upper and lower lines correspond to the earlier and later times, respectively). Closed circles indicate the point $[\xi(t),\zeta(t)]$ at the three different times. In the liquid region ($x<\xi$) the profile is expressed as Eq. (21) and in the gel region ($\xi \le x<1$) it is a part of the trajectory of $[\xi(t),\zeta(t)]$.

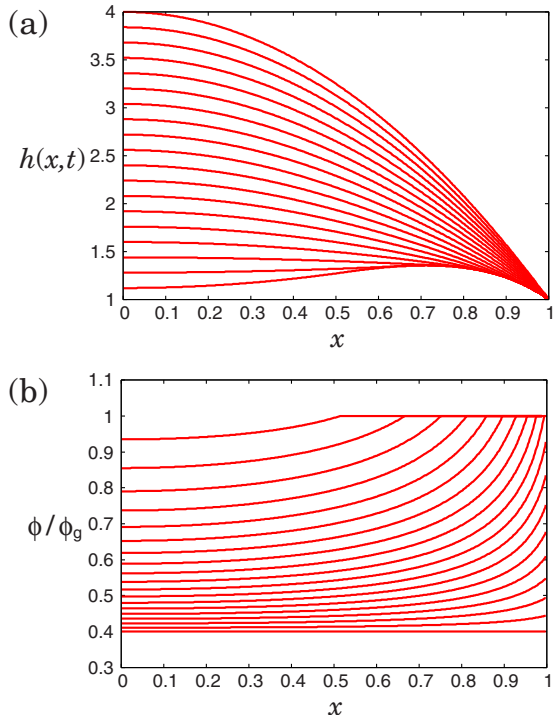

FIG. 4. (Color online) Time evolution of the height and the concentration distribution obtained by the numerical simulation of the simplified model for the initial values $(\phi_0/\phi_g, b_0)=(0.4,4)$ in the absence of diffusion. (a) Profiles of $h(x,t)$ at several times are plotted as functions of x. The time increases from the top line to the bottom line. (b) Profiles of $\phi(x,t)$ at several times are plotted as functions of x. The time increases from the bottom line to the top line.

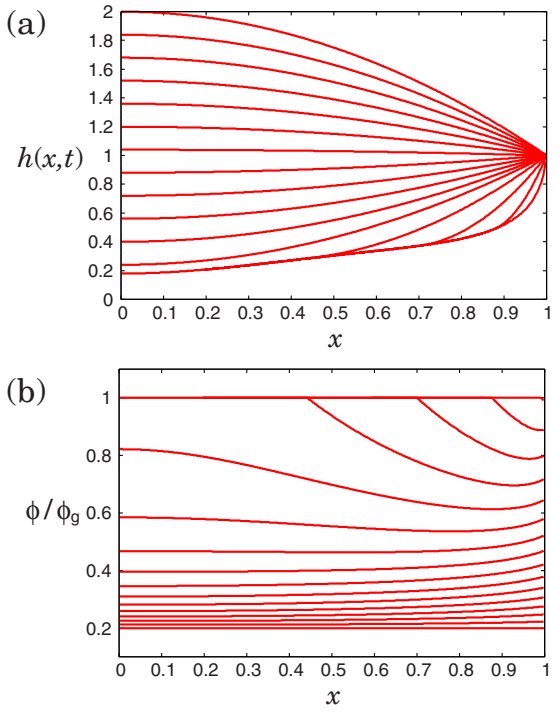

FIG. 5. (Color online) Time evolution of the height and the concentration distribution obtained by the numerical simulation of the simplified model for the initial values $(\phi_0/\phi_g, b_0)=(0.2,2)$ in the absence of diffusion. (a) Profiles of $h(x,t)$ at several times are plotted as functions of x. The times increase from the top line to the bottom line. (b) Profiles of $\phi(x,t)$ at several times are plotted as functions of x. The time increases from the bottom line to the top line.

$$\left.\frac{\partial h}{\partial x}\right|_{x=\xi(t)} = \frac{\dot{\zeta}(t)}{\dot{\xi}(t)}, \tag{28}$$

where $\dot{\xi} \equiv d\xi/dt$ and $\dot{\zeta} \equiv d\zeta/dt$. This means that the profile $h(x,t)$ in the liquid region is smoothly connected to the trajectory of $[\xi(t), \zeta(t)]$ at the gelation front.

In Fig. 4 we show the profiles of $h(x,t)$ and $\phi(x,t)$ at several times for the initial values $(\phi_0/\phi_g, b_0)=(0.4,4)$. We can see that after rapid increase in ϕ near $x=1$ the gelation starts at $x=1$ and the final shape which has a peak in $0<x<1$ appears. In the case that both ϕ_0/ϕ_g and b_0 are small, we observe that the gelation starts at $x=0$ (Fig. 5). This is not the case that another type of final shape arises, although the observed shape is a little distorted. In the following analysis we do not consider this case.

Figure 6 shows the parameter dependence of final shape. We observe three types of the shape: (i) the shapes of monotonically increasing in x ("basin type"), having a peak in $0<x<l_0$ ("crater type"), and monotonically decreasing in x ("mound type"), depending on the initial parameters $(\phi_0/\phi_g, b_0)$.

2. Pregelation regime

Here we analyze theoretically the dynamics in the pregelation regime described by Eqs. (7) and (23)–(27) with $\xi=\zeta=1$. Equation (23) and the initial condition $\phi(x,0)=\phi_0$ form an initial value problem of a linear partial differential equation, which can be solved by the method of characteristics [47] as follows. Consider a curve parametrized by τ in (x,t) space. The total differentiation of $\phi=\phi(x,t)$ along this curve is given as

$$\frac{d\phi}{d\tau} = \frac{\partial\phi}{\partial x}\frac{dx}{d\tau} + \frac{\partial\phi}{\partial t}\frac{dt}{d\tau}. \tag{29}$$

Comparing this with Eq. (23) we obtain a set of ordinary differential equations as

$$\frac{dt}{d\tau} = h(x,t), \tag{30}$$

$$\frac{dx}{d\tau} = Q(x,t), \tag{31}$$

$$\frac{d\phi}{d\tau} = \phi. \tag{32}$$

Since there is a unique solution of Eqs. (30)–(32) for a given set of the initial values which we put $(x,t,\phi)=(s,0,\phi_0)$ at $\tau=0$ with $0\le s\le 1$, a set of the characteristic curves (trajectories of the solution) with the parameter s forms a surface $\phi=\phi(s,\tau)$ in (s,τ,ϕ) space. The parameters s and τ can be

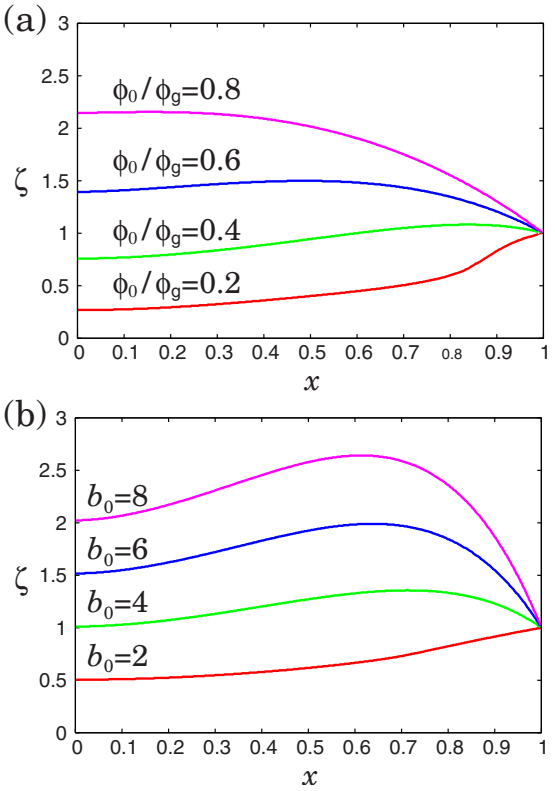

FIG. 6. (Color online) Initial parameter dependence of the final shapes obtained by the numerical simulation of the simplified model in the absence of diffusion. (a) The final shapes ζ are plotted as functions of x for the initial values $(\phi_0/\phi_g, b_0)=(0.2, 3)$, (0.4, 3), (0.6, 3), and (0.8, 3) from the bottom line to the top line. (b) The final shapes ζ are plotted as functions of x for the initial values $(\phi_0/\phi_g, b_0)=(0.4, 2)$, (0.4, 4), (0.4, 6), and (0.4, 8) from the bottom line to the top line.

considered as independent coordinates in (x,t) space, if the mapping $s=s(x,t)$ and $\tau=\tau(x,t)$ is unique. Therefore, if such mapping exists, we can obtain $\phi=\phi(x,t)$ as a function of x and t which should coincide with a solution of Eq. (23). In Fig. 7 we plot several curves of $s(x,t)=$const and $\tau(x,t)=$const obtained from Eqs. (33) and (34) below.

Equations (30)–(32) can be understood, physically, as follows. Imagine the motion of a fluid element with volume (or area) $h(x,t)\Delta x$ at position $x(t)$ and time t. The element moves along the flow with a speed Q/h, i.e., $dx/dt=Q/h$. The volume of element is decreasing in time due to the evaporation: $d(h\Delta x)/dt=-J\Delta x$, whereas the amount of polymers is conserved: $d(\phi h\Delta x)/dt=0$, which leads to $d\phi/dt=J\phi/h$. Introducing τ as $dt=hd\tau$, we obtain Eqs. (30)–(32).

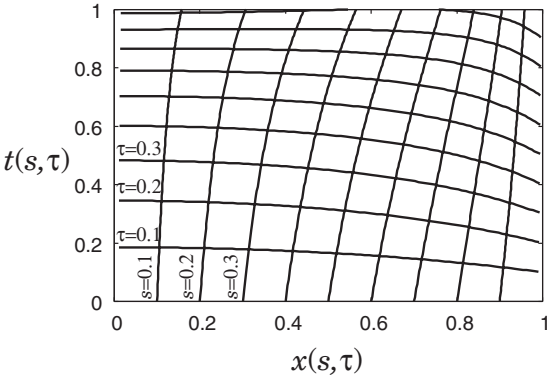

FIG. 7. Plots of curves $s(x,t)=$const and $\tau(x,t)=$const obtained from Eqs. (33) and (34) with $a_0=1$.

Now we solve Eqs. (30)–(32) for the initial values: $t=0$, $x=s$, and $\phi=\phi_0$ at $\tau=0$. We obtain $t=t(s,\tau)$, $x=x(s,\tau)$, and $\phi=\phi(s,\tau)$ as functions of s and τ:

$$t(s,\tau)=\frac{2}{3}a_0\left[1-\left(\frac{s}{x}\right)^3\right]-\frac{1}{x^3}\left[2(x-s)+\ln\frac{1-x}{1+x}-\ln\frac{1-s}{1+s}\right], \tag{33}$$

$$x(s,\tau)=s[s^2+(1-s^2)e^{-\tau}]^{-1/2}, \tag{34}$$

and

$$\phi(s,\tau)=\phi_0 e^{\tau}. \tag{35}$$

The last equation ensures that $\phi(s,\tau)>0$. This is obvious physically, because the concentration of a fluid element always increases under the positive evaporation of the solvent $(J_0>0)$ until ϕ reaches ϕ_g where the evaporation rate vanishes. Note that t is an increasing function of τ as long as $h>0$ and that at $s=0$ and 1 we have

$$t(0,\tau)=\frac{2}{3}b_0(1-e^{-3\tau/2}), \tag{36}$$

$$t(1,\tau)=\tau. \tag{37}$$

The time $t_f\equiv\lim_{\tau\to\infty}t(0,\tau)=2b_0/3$ corresponds to the time when h at $x=0$ approaches 0, i.e., $h(0,t_f)=0$.

If we can eliminate τ and s from Eqs. (33)–(35), we obtain ϕ as a function of x and t. Unfortunately, we cannot perform that analytically but only numerically. However, we can know behaviors of ϕ at special points $x=0$ and 1 analytically. We find

$$\phi(0,t)=\phi_0\left[\frac{b(t)}{b_0}\right]^{-2/3}, \tag{38}$$

$$\phi(1,t)=\phi_0 e^{t}. \tag{39}$$

Equations (38) and (39) suggest that the gelation will start at $x=0$ or 1 depending on the value of b_0. There is a cross point (ϕ^*,t^*) defined as $\phi(0,t^*)=\phi(1,t^*)=\phi^*$ $(t^*>0)$. If $\phi^*>\phi_g$, the gelation takes place at $x=1$, otherwise it takes place at $x=0$. In Fig. 8 we show the parameter regions in $(\phi_0/\phi_g, b_0)$ plane where the gelation starts at $x=0$ (lower region) or 1 (upper region).

3. Postgelation regime

In the postgelation regime $t>t_g$, where the gelation time t_g is defined as $t_g\equiv\ln(\phi_g/\phi_0)$, the time evolution of the system is described by Eq. (23) with Eqs. (21) and (25)–(27). We should solve Eq. (23) in $0<x<\xi(t)$ for the initial value $\phi(x,0)=\tilde{\phi}(x)$ which is the concentration profile when ϕ at $x=1$ reaches ϕ_g. Hereafter we shift the origin of time so that

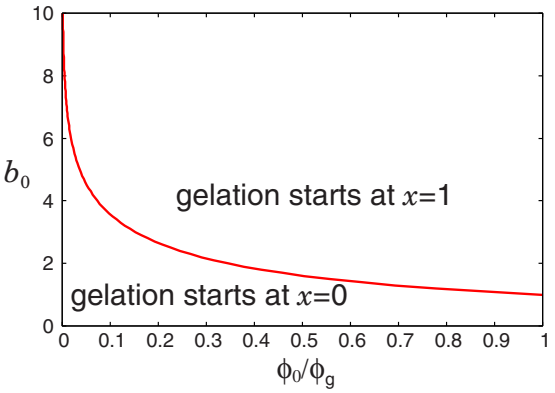

FIG. 8. (Color online) Parameter regions in $(\phi_0/\phi_g, b_0)$ plane where the gelation starts at $x=0$ (lower region) or 1 (upper region).

the gelation starts at $t=0$. It is hard to solve this problem analytically, since in order to solve Eq. (23) we need information on the position $\xi(t)$ and the height $\zeta(t)$ of the gelation front which should be determined by solving the equation itself. In the following we discuss about a final shape of the film by analyzing a trajectory of $[\xi(t), \zeta(t)]$.

Consider the motion of a fluid element starting from $x=s$ at $t=\tau=0$ which is described by Eqs. (30)–(32) for the postgelation model where h and Q in these equations now depend on $\xi(t)$ and $\zeta(t)$. Position of the fluid element $x(s,\tau)$ can be obtained from Eq. (31) with Eq. (26) as

$$\frac{1}{x^2(s,\tau)} = \frac{e^{-\tau}}{s^2} + \int_0^\tau d\tau' \frac{e^{-(\tau-\tau')}}{\xi^2(t(s,\tau'))}, \tag{40}$$

provided that $\xi(t)$ is given. From Eq. (32) we have

$$\phi(s,\tau) = \tilde{\phi}(s)e^{\tau} \tag{41}$$

with the initial concentration profile $\tilde{\phi}(s)$. Hence the fluid element becomes a gel at $\tau=\tau_g(s)$, where

$$\tau_g(s) \equiv \ln\left[\frac{\phi_g}{\tilde{\phi}(s)}\right]. \tag{42}$$

Since $x(s,\tau_g(s))$ should be equal to $\xi(t(s,\tau_g(s)))$, we have the integral equation for ξ as

$$\frac{1}{\xi^2(t(s,\tau_g))} = \frac{e^{-\tau_g}}{s^2} + \int_0^{\tau_g} d\tau' \frac{e^{-(\tau_g-\tau')}}{\xi^2(t(s,\tau'))}. \tag{43}$$

If we make a rough approximation that $t(s,\tau)$ does not depend on s, namely, $h(x,t)$ is only a function of t [see Eq. (30)], we can transform Eq. (43) into the differential equation as

$$\frac{d\xi}{ds} = \left(\frac{\xi}{s}\right)^3 \frac{\tilde{\phi}(s)}{\phi_g}, \tag{44}$$

where ξ is a function of s through $\tau_g(s)$. A solution of Eq. (44) which satisfies the condition that $\xi=1$ at $s=1$ is

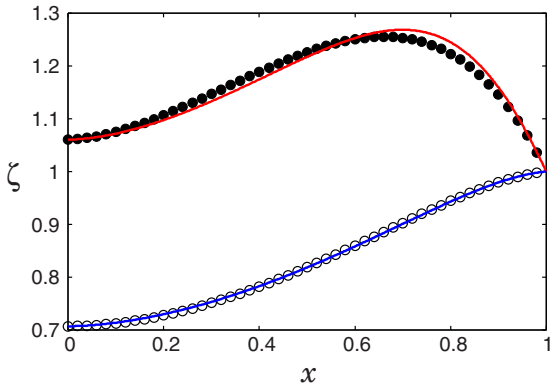

FIG. 9. (Color online) Comparison of the theoretical curves for the film profiles with the numerical data. The theoretical curves for $(\phi_0/\phi_g, b_0)=(0.5,2)$ and $(0.5,3)$ are plotted with the lower and upper solid lines, respectively. The numerical data for $(\phi_0/\phi_g, b_0)=(0.5,2)$ and $(0.5,3)$ are indicated with the open and closed circles.

$$\xi(s) = \left[1 + 2\int_s^1 ds' \frac{\tilde{\phi}(s')}{s'^3\phi_g}\right]^{-1/2}. \tag{45}$$

Since ζ can be regarded as a function of the coordinate x, the mass conservation Eq. (2) with $D=0$ implies

$$\int_s^1 ds' \tilde{\phi}(s')\tilde{h}(s') = \int_{\xi(s)}^1 dx \phi_g \zeta(x), \tag{46}$$

where

$$\tilde{h}(s) = -\tilde{a}_0 s^2 + \tilde{b}_0 \tag{47}$$

is the initial shape of the film with $\tilde{a}_0 \equiv a_0 - (3/2)t_g$ and $\tilde{b}_0 \equiv b_0 - (3/2)t_g$. Differentiating Eq. (46) with respect to s and using Eq. (44), we obtain ζ as a function of s,

$$\zeta(s) = \left(\frac{s}{\xi}\right)^3 \tilde{h}(s). \tag{48}$$

Equations (45) and (48) for $0<s<1$ give a parametric expression of a final shape of the film.

In Fig. 9 we show the final shapes of the film given by Eqs. (45) and (48), where the initial profiles of concentration $\tilde{\phi}(s)$ are obtained by solving Eqs. (33)–(35), numerically, for the initial values $(\phi_0/\phi_g, b_0)=(0.5,2.0)$ and $(0.5,3.0)$. We also plot in the same figure the data obtained by numerical simulations of Eqs. (21), (23), and (25)–(27) for the same parameters as above. The theoretical expressions well fit the numerical data for the case that $\tilde{h}(s)$ is nearly constant in s $(\tilde{a}_0 \simeq 0)$ as expected. Although the theoretical curves deviate from the numerical data for $\tilde{a}_0 \neq 0$, the qualitative feature of the curves, namely, the shapes coincide between them. Indeed the "phase boundary" related to the shape change in the parameter space $(\phi_0/\phi_g, b_0)$ (Fig. 10) is not affected by the above approximation.

4. Final shape

Now we can discuss the initial parameter dependence of the final shape expressed as Eqs. (45) and (48). In the fol-

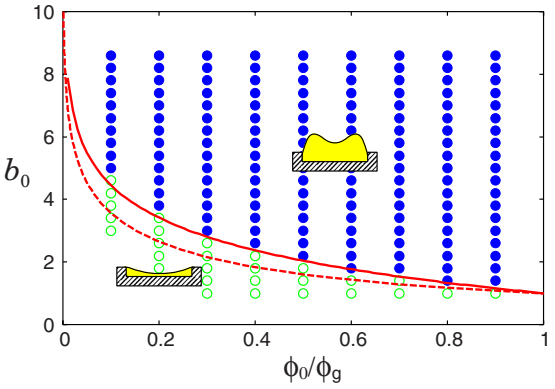

FIG. 10. (Color online) The shape diagram showing the initial parameter dependence of the final shape in the absence of diffusion. The theoretical curve (solid line) is compared with the numerical data (open and closed circles) in the parameter space $(\phi_0/\phi_g, b_0)$. Open or closed circles indicate the values of parameters $(\phi_0/\phi_g, b_0)$ for which the final shape of the film is basin type or crater type, respectively. Here b_0 is the initial height of the film scaled by h_0, that is, $b(0)/h_0$ using the expression of Eq. (16). The dashed line is the same curve as shown in Fig. 8 below which the gelation starts at $x=0$.

lowing, we only consider the case that $d\tilde{\phi}/ds>0$ for $0<s<1$. In order to know a qualitative shape of the deposit, it is enough to discuss the functional form of ζ as a function of s instead of that as a function of ξ, since $d\xi/ds>0$ as shown in Eq. (44). From Eq. (45) we can show that $(s/\xi)^3$ is a monotonically increasing function of s for $0<s<1$. Therefore Eq. (48) suggests that there are three types of the shape: (i) $\zeta(s)$ is monotonically increasing, (ii) $\zeta(s)$ has a maximum point in $0<s<1$, and (iii) $\zeta(s)$ is monotonically decreasing, corresponding to the basin, crater, and mound types, respectively, as obtained by the numerical simulations. The parameter region in which one of the above three types appears is determined as follows. When $\tilde{a}_0 \leq 0$, or equivalently,

$$b_0 \leq 1 - \frac{3}{2}\ln\frac{\phi_0}{\phi_g}, \tag{49}$$

$\tilde{h}(s)$ is not decreasing in $0<s<1$. In this region the shape of basin type will appear. When $\hat{a}_0>0$, $\tilde{h}(s)$ is a decreasing function and $\zeta(s)$ has a maximum point in $0\leq s<1$. The last statement can be shown as follows. From Eq. (48) $\zeta(s)$ has an extremum at $s=s^*$ which is a solution of the equation

$$\frac{g'}{g} + \frac{\tilde{h}'}{\tilde{h}} = 0, \tag{50}$$

with $g(s)\equiv(s/\xi)^3$, $g'\equiv dg/ds$, and $\tilde{h}'\equiv d\tilde{h}/ds$. Since $g'(s)>0$ for $0<s<1$, $g'(0)=g'(1)=0$, $\tilde{h}'(s)<0$ for $0<s\leq 1$, $\tilde{h}'(0)=0$, and $g''(0)=\infty$ provided that $\tilde{\phi}''(0)>0$, Eq. (50) has two solutions $s=0$ and s^* with $0<s^*<1$. Furthermore, we can show that $\zeta'(1)<0$. Therefore, $\zeta(s)$ takes a maximum at $s=s^*$, that is, the shape of crater type appears if $\tilde{a}_0<0$. The shape of mound type will not appear in this model except for the case that $\xi=s$, namely, $\tilde{\phi}(s)=\phi_g$, and $\tilde{a}_0>0$.

In Fig. 10 we show the initial parameter dependence of the final shape, which we call shape diagram, obtained by the above theoretical analysis together with the result of the numerical simulations. The theoretical prediction agrees well with the numerical result, as expected. These results are consistent with the experimental results [43].

The dashed line in Fig. 10 is the same curve as shown in Fig. 8 below which the gelation starts at $x=0$. This curve is always below the theoretical phase boundary (solid line), which implies that the phase boundary is not affected by whether gelation starts at $x=0$ or 1. However, we observe that the numerical data slightly deviate from the theoretical curve (solid line) at small ϕ_0/ϕ_g. This is due to the fact that in that region the gelation fronts appear from both sides (see Appendix A). Although the theoretical analysis cannot be applied for such complicated situations, the shapes of final deposits obtained numerically are not so largely deformed from those in the normal cases.

B. Effect of diffusion

In the presence of diffusion $(D\neq 0)$ it is hard to perform a theoretical analysis. Here we carry out the numerical simulation of our model with a finite diffusion constant D, or a finite Péclet number Pe, and discuss effects of diffusion on the final shape of the film. The numerical method is the same as before except that now we solve

$$h\frac{\partial\phi}{\partial t} + Q\frac{\partial\phi}{\partial x} = \mathrm{Pe}^{-1}\,\epsilon\frac{\partial}{\partial x}\left(h\frac{\partial\phi}{\partial x}\right) + J\phi, \tag{51}$$

instead of Eq. (23) under the boundary conditions $\partial\phi/\partial x=0$ at $x=0$ and 1, where the Péclet number Pe and the aspect ratio of the bank geometry ϵ are given as

$$\mathrm{Pe} \equiv \frac{J_0 l_0}{D} \quad \text{and} \quad \epsilon \equiv \frac{h_0}{l_0}. \tag{52}$$

In Fig. 11 we show the shape diagrams for $\mathrm{Pe}^{-1}\,\epsilon=0.01$ and 1. We can see that the parameter region of basin type becomes wider as $\mathrm{Pe}^{-1}\,\epsilon$ is larger and the region of mound type appears for $\mathrm{Pe}^{-1}\,\epsilon=1$, which never appears in the absence of diffusion. This result is reasonable because the diffusion tends to homogenize the concentration field $\phi(x,t)$ contrary to the outward flow which causes inhomogeneous distribution of $\phi(x,t)$ under the solvent evaporation. Since $\mathrm{Pe}^{-1}\,\epsilon$ gives an estimate of degree of the diffusion flux relative to the flow in this system, the diffusion process dominates the dynamics of drying process when $\mathrm{Pe}^{-1}\,\epsilon>1$, which gives rise to appearing the shape of mound type.

IV. BANKLESS SUBSTRATE

Here we discuss the shape of deposit without bank geometry. We assume that the contact line is still pinned even if there is no bank. This situation corresponds to the case $h_0=0$ in our model. In this case we can obtain the explicit form of $\phi(x,t)$ in the pregelation regime as, using the dimensionless variables,

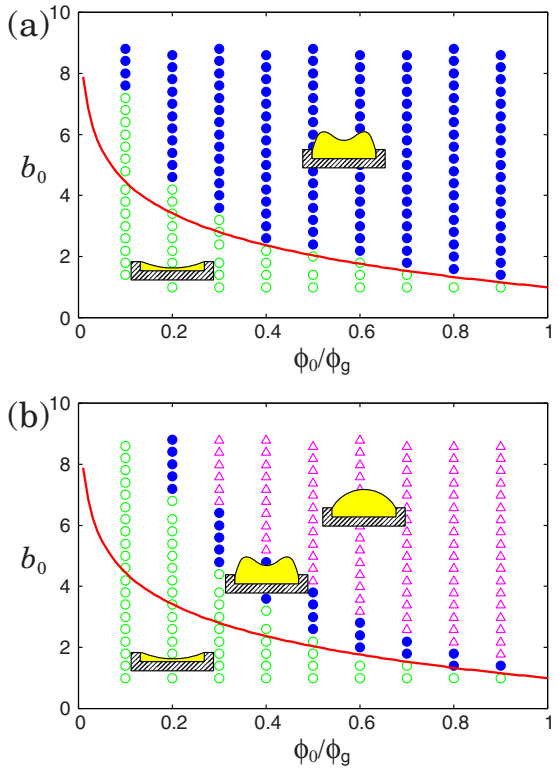

FIG. 11. (Color online) The shape diagram showing the initial parameter dependence of the final shape obtained by the numerical simulations for Pe^{-1} $\epsilon=0.01$ (a) and 1 (b). Open circles, closed circles, and triangles indicate the values of parameters $(\phi_0/\phi_g, b_0)$ for which the final shape of the film is basin type, crater type, and mound type, respectively. The solid line is the theoretical curve below or above which the shape of basin type or crater type appears in the absence of diffusion.

$$\phi(x,t) = \phi_0 \frac{b^{-2/3}(t) - x^2}{1 - x^2}, \tag{53}$$

where $b(t)$ is given by

$$b(t) = 1 - \frac{3}{2}t. \tag{54}$$

Here we have chosen the initial height of the film b_0 as a unit of space in z direction instead of h_0 and b_0/J_0 as a unit of time. Equation (53) shows that $\phi(x,t)$ diverges at $x=1$ for $t>0$. This implies that the gelation starts on the contact line at $t=0$.

Using Eqs. (45) and (48) with $\tilde{\phi}(s)=\phi_0$, we obtain the final shape ζ as a function of ξ,

$$\zeta = \frac{\Phi^{-1}(1-\xi^2)}{[\xi^2 + \Phi^{-1}(1-\xi^2)]^{5/2}}, \tag{55}$$

where $\Phi \equiv \phi_0/\phi_g$. Since a profile of the film is scaled by its initial height b_0, Eq. (55) includes only one parameter Φ. The profile of $\zeta(\xi)$ changes depending on the value of Φ. We can show that if $\Phi<3/5$, $\zeta(\xi)$ has a crater-type shape, otherwise, it has a mound-type shape. In Fig. 12 we show the functional forms of $\zeta(\xi)$ given by Eq. (55) for a few values of Φ.

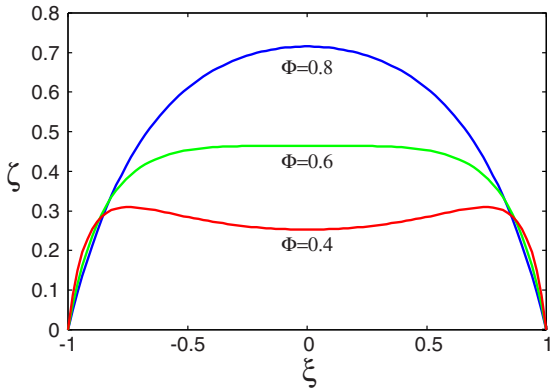

FIG. 12. (Color online) Functional forms $\zeta(\xi)$ given by Eq. (55) for $\Phi=0.4$, 0.6, and 0.8.

V. CONCLUDING REMARKS

In this paper we have proposed a simple model which describes the drying processes of polymer solutions on a substrate taking into account the gelation of the solutions in the limit of $\mathrm{Ca}\to 0$. We have analyzed theoretically the model to predict a final shape of the film in the bank geometry. In the absence of diffusion ($\mathrm{Pe}\to\infty$), there are two parameters in our model which are the initial polymer concentration relative to the gelation concentration, ϕ_0/ϕ_g, and the initial height of the film relative to the height of the bank, b_0/h_0. We have obtained theoretical expressions Eqs. (45) and (48) for the final shape of the film in terms of the concentration and the film profiles when the gelation starts at the edge of the film. The final shape is determined by the initial parameters ϕ_0/ϕ_g and b_0/h_0. Depending on these parameters, two types of the final shape appear which are the basin type and the crater type. The boundary between the parameter regions in which the basin-type shape and the crater-type shape appear is given by Eq. (49). These theoretical predictions qualitatively agree with the experimental results [43]. In the presence of diffusion, we have shown numerically that the region of the crater-type shape becomes narrower and the region of the mound-type shape appears for large Pe^{-1}. We have discussed the final shape of the film in the geometry without bank. In this geometry ϕ_0/ϕ_g is the only parameter which determines the final shape in the absence of diffusion and has a critical value above (below) which the mound-type (crater-type) shape appears.

We believe that these results give basic information for some practical applications. In this paper we do not consider the following cases: (i) Ca is finite; (ii) the solvent evaporation rate depends on the distribution of the solvent in the gas phase surrounding the liquid films or droplets. These will be important subjects in the future.

ACKNOWLEDGMENTS

This work was supported by JSPS KAKENHI (Grant No. 18540403) and KAKENHI (Grant-in-Aid for Scientific Re-

search) on Priority Area "Soft Matter Physics" from the Ministry of Education, Culture, Sports, Science and Technology of Japan.

APPENDIX A: EXTENDED MODEL

In the model shown in Sec. II we have assumed that the gel-like phase begins to develop only from the edge ($x=l_0$) of the system. However, it may develop also from the center ($x=0$). In order to carry out numerical simulations in both cases, we extend our model as follows. Let ξ_0 and ξ_1 be the positions of the gel fronts propagating from the center to the edge and the edge to the center, respectively. Assume that $\phi(x,t)=\phi_g$ and $Q(x,t)=0$ in the gel region $0\leq x\leq \xi_0$ and $\xi_1\leq x\leq l_0$ and that the film profile $h(x,t)$ in $\xi_0<x<\xi_1$ has the following form:

$$h(x,t) = -a(t)x^2 + c(t)x + b(t). \tag{A1}$$

The same argument as in Sec. II leads to

$$Q(x,t) = -\frac{J_0}{(\xi_1-\xi_0)^2}(x-\xi_0)(x-\xi_1)(2x-\xi_0-\xi_1) \tag{A2}$$

for $\xi_0<x<\xi_1$,

$$\frac{da}{dt} = -\frac{6J_0}{(\xi_1-\xi_0)^2}, \tag{A3}$$

$$b = \zeta_1 + a\xi_1^2 - c\xi_1, \tag{A4}$$

and

$$c = a(\xi_0+\xi_1) + \frac{\zeta_1-\zeta_0}{\xi_1-\xi_0}, \tag{A5}$$

where $\zeta_0 \equiv h(\xi_0,t)$ and $\zeta_1 \equiv h(\xi_1,t)$. We can numerically solve Eq. (4) with Eqs. (A1)–(A5) under the same boundary conditions as before.

APPENDIX B: AXIAL SYMMETRIC SYSTEM

For the system with the axial symmetry we can perform a theoretical analysis with the same argument as shown in Sec. III. Here we show the main results.

Consider the system created by the rotation of the system shown in Fig. 1 around z axis. In this system $h=-a(t)r^2+b(t)$ now expresses a paraboloid of revolution, where r is the radial coordinate. The conservation laws in the absence of diffusion are now written, in the dimensionless form, as

$$\frac{\partial h}{\partial t} + \frac{1}{r}\frac{\partial}{\partial r}(rQ) = -J, \tag{B1}$$

$$h\frac{\partial \phi}{\partial t} + Q\frac{\partial \phi}{\partial r} = J\phi. \tag{B2}$$

Assuming that

$$h(r,t) = (b-\zeta)\left(1-\frac{r^2}{\xi^2}\right) + \zeta, \tag{B3}$$

$$J(r,t) = \begin{cases} 1 & [0\leq r<\xi(t)] \\ 0 & [\xi(t)\leq r\leq 1], \end{cases} \tag{B4}$$

we have

$$b(t) = b_0 - 2t, \tag{B5}$$

$$Q(r,t) = \begin{cases} \dfrac{r}{2}\left(1-\dfrac{r^2}{\xi^2}\right) & [0\leq r<\xi(t)] \\ 0 & [\xi(t)\leq r\leq 1]. \end{cases} \tag{B6}$$

In the pregelation regime ($\xi=\zeta=1$), we can solve Eq. (B2) for the initial condition $\phi(r,0)=\phi_0$ under the boundary condition $\partial\phi/\partial r=0$ at $r=0$ using the same method as in Sec. III. We obtain, as counterparts of Eqs. (33)–(35),

$$t(s,\tau) = \frac{a_0}{2}\left[1-\left(\frac{s}{r}\right)^4\right] - \frac{1}{r^4}\left[r^2-s^2+\ln\left(\frac{r^2}{s^2}\right)-\tau\right], \tag{B7}$$

$$r(s,\tau) = s[s^2+(1-s^2)e^{-\tau}]^{-1/2}, \tag{B8}$$

$$\phi(s,\tau) = \phi_0 e^{\tau}. \tag{B9}$$

At $r=0$ and 1, we have

$$\phi(0,\tau) = \phi_0\left[\frac{b(t)}{b_0}\right]^{-1/2}, \tag{B10}$$

$$\phi(1,\tau) = \phi_0 e^{t}. \tag{B11}$$

In the postgelation regime, we have the same expression as Eq. (45) for $\xi(s)$. Since the mass conservation Eq. (46) now becomes

$$\int_s^1 ds' 2\pi s' \tilde{\phi}(s')\tilde{h}(s') = \int_{\xi(s)}^1 dr 2\pi r \phi_g \zeta(r), \tag{B12}$$

we obtain

$$\zeta(s) = \left(\frac{s}{\xi}\right)^4 \tilde{h}(s), \tag{B13}$$

where $\tilde{h}(s)$ is given by Eq. (47) with $\tilde{a}_0 \equiv a_0 - 2t_g$ and $\tilde{b}_0 \equiv b_0 - 2t_g$.

The phase boundary between the basin-type shape and the crater-type shape in the initial parameter space is now given by

$$b_0 = 1 - 2\ln\frac{\phi_0}{\phi_g}. \tag{B14}$$

For the geometry without bank the concentration profile is obtained as

$$\phi(r,t) = \phi_0\frac{b^{-1/2}(t)-r^2}{1-r^2}, \tag{B15}$$

instead of Eq. (53), where $b(t)$ is given by

$$b(t) = 1 - 2t. \tag{B16}$$

The final shape of the film is obtained as

$$\zeta = \frac{\Phi^{-1}(1-\xi^2)}{[\xi^2 + \Phi^{-1}(1-\xi^2)]^3}. \tag{B17}$$

The critical value of Φ at which the final shape changes from the crater type to the mound type is 2/3.

[1] R. D. Deegan, O. Bakajin, T. F. Dupont, G. Huber, S. R. Nagel, and T. A. Witten, Nature (London) **389**, 827 (1997).
[2] R. D. Deegan, O. Bakajin, T. F. Dupont, G. Huber, S. R. Nagel, and T. A. Witten, Phys. Rev. E **62**, 756 (2000).
[3] Y. O. Popov and T. A. Witten, Eur. Phys. J. E **6**, 211 (2001).
[4] Y. O. Popov and T. A. Witten, Phys. Rev. E **68**, 036306 (2003).
[5] B. Rieger, L. R. van den Doel, and L. J. van Vliet, Phys. Rev. E **68**, 036312 (2003).
[6] M. Tsige and G. S. Grest, Macromolecules **37**, 4333 (2004).
[7] R. Zheng, Y. O. Popov, and T. A. Witten, Phys. Rev. E **72**, 046303 (2005).
[8] G. Li, H.-J. Butt, and K. Graf, Langmuir **22**, 11395 (2006).
[9] T. Kajiya, D. Kaneko, and M. Doi, Langmuir **24**, 12369 (2008).
[10] C. Poulard, G. Guéna, A. M. Cazabat, A. Boudaoud, and M. Ben Amar, Langmuir **21**, 8226 (2005).
[11] E. Rio, A. Daerr, F. Lequeux, and L. Limat, Langmuir **22**, 3186 (2006).
[12] G. Berteloot, C.-T. Pham, A. Daerr, F. Lequeux, and L. Limat, Europhys. Lett. **83**, 14003 (2008).
[13] C. Monteux, Y. Elmaallem, T. Narita, and F. Lequeux, Europhys. Lett. **83**, 34005 (2008).
[14] S. Maheshwari, L. Zhang, Y. Zhu, and H.-C. Chang, Phys. Rev. Lett. **100**, 044503 (2008).
[15] E. Adachi, A. S. Dimitrov, and K. Nagayama, Langmuir **11**, 1057 (1995).
[16] R. D. Deegan, Phys. Rev. E **61**, 475 (2000).
[17] Y. Yamazaki and T. Mizuguchi, J. Phys. Soc. Jpn. **69**, 2387 (2000).
[18] E. Bormashenko, R. Pogreb, O. Stanevsky, Y. Bormashenko, T. Stein, V.-Z. Gaisin, R. Cohen, and O. V. Gendelman, Macromol. Mater. Eng. **290**, 114 (2005).
[19] Y. Gotkis, I. Ivanov, N. Murisic, and L. Kondic, Phys. Rev. Lett. **97**, 186101 (2006).
[20] M. H. Eres, D. E. Weidner, and L. W. Schwartz, Langmuir **15**, 1859 (1999).
[21] P. G. de Gennes, Eur. Phys. J. E **6**, 421 (2001).
[22] H. Hu and R. G. Larson, Langmuir **21**, 3972 (2005).
[23] E. Sultan, A. Boudaoud, and M. B. Amar, J. Fluid Mech. **543**, 183 (2005).
[24] C. Poulard and P. Damman, Europhys. Lett. **80**, 64001 (2007).
[25] D. J. Harris and J. A. Lewis, Langmuir **24**, 3681 (2008).
[26] P. G. de Gennes, Eur. Phys. J. E **7**, 31 (2002).
[27] K. Ozawa, T. Okuzono, and M. Doi, Jpn. J. Appl. Phys., Part 1 **45**, 8817 (2006).
[28] T. Okuzono, K. Ozawa, and M. Doi, Phys. Rev. Lett. **97**, 136103 (2006).
[29] T. Okuzono and M. Doi, Phys. Rev. E **77**, 030501(R) (2008).
[30] L. Pauchard and C. Allain, Europhys. Lett. **62**, 897 (2003).
[31] L. Pauchard and C. Allain, Phys. Rev. E **68**, 052801 (2003).
[32] T. Kajiya, E. Nishitani, T. Yamaue, and M. Doi, Phys. Rev. E **73**, 011601 (2006).
[33] D. A. Head, Phys. Rev. E **74**, 021601 (2006).
[34] D. E. Bornside, C. W. Macosko, and L. E. Scriven, J. Appl. Phys. **66**, 5185 (1989).
[35] A. F. Routh and W. B. Russel, AIChE J. **44**, 2088 (1998).
[36] P. L. Evans, L. W. Schwartz, and R. V. Roy, J. Colloid Interface Sci. **227**, 191 (2000).
[37] B.-J. de Gans and U. S. Schubert, Langmuir **20**, 7789 (2004).
[38] D. Soltman and V. Subramanian, Langmuir **24**, 2224 (2008).
[39] H. Hu and R. G. Larson, J. Phys. Chem. B **106**, 1334 (2002).
[40] H. Hu and R. G. Larson, Langmuir **21**, 3963 (2005).
[41] K. Ozawa, E. Nishitani, and M. Doi, Jpn. J. Appl. Phys., Part 1 **44**, 4229 (2005).
[42] J. Fukai, H. Ishizuka, Y. Sakai, M. Kaneda, M. Morita, and A. Takahara, Int. J. Heat Mass Transfer **49**, 3561 (2006).
[43] Y. Jung, T. Kajiya, T. Yamaue, and M. Doi, Jpn. J. Appl. Phys. **48**, 031502 (2009).
[44] R. Teshigawara and A. Onuki, Europhys. Lett. **84**, 36003 (2008).
[45] A. Oron, S. H. Davis, and S. G. Bankoff, Rev. Mod. Phys. **69**, 931 (1997).
[46] M. Kobayashi, M. Makino, T. Okuzono, and M. Doi (unpublished).
[47] S. J. Farlow, *Partial Differential Equations for Scientists and Engineers* (Dover, New York, 1993).